Identifying the potential therapeutic effects of miR-6516 on muscle disuse atrophy

WOOHYEONG JUNG[1,2], UIJIN JUANG[1,2], SUHWAN GWON[1,2], HOUNGGIANG NGUYEN[1,2],
QINGZHI HUANG[1,2], SOOHYEON LEE[1,2], BEOMWOO LEE[1,2], SEON-HWAN KIM[3],
SUNYOUNG RYU[4], JISOO PARK[4] and JONGSUN PARK[1,2,4]

Departments of [1]Pharmacology and [2]Medical Science, College of Medicine, Chungnam National University;
[3]Department of Neurosurgery, Institute for Cancer Research, College of Medicine, Chungnam National University,
Daejeon 35015; [4]Mitos Biomedical Institute, Mitos Therapeutics Inc., Daejeon 34134, Republic of Korea

Abstract. Muscle atrophy is a debilitating condition with various causes; while aging is one of these causes, reduced engagement in routine muscle-strengthening activities also markedly contributes to muscle loss. Although extensive research has been conducted on microRNAs (miRNAs/miRs) and their associations with muscle atrophy, the roles played by miRNA precursors remain underexplored. The present study detected the upregulation of the miR-206 precursor in cell-free (cf)RNA from the plasma of patients at risk of sarcopenia, and in cfRNAs from the muscles of mice subjected to muscle atrophy. Additionally, a decline in the levels of the miR-6516 precursor was observed in mice with muscle atrophy. The administration of mimic-miR-6516 to mice immobilized due to injury inhibited muscle atrophy by targeting and inhibiting cyclin-dependent kinase inhibitor 1b (*Cdkn1b*). Based on these results, the miR-206 precursor appears to be a potential biomarker of muscle atrophy, whereas miR-6516 shows promise as a therapeutic target to alleviate muscle deterioration in patients with muscle disuse and atrophy.

Introduction

Sarcopenia refers to the gradual loss of muscle mass and muscle strength, and the main symptoms are muscle loss and weakness (1,2). Although sarcopenia is mainly a disease of elderly individuals, it can be associated with diseases that are not confined to the elderly population. Muscle reduction syndrome is characterized by a gradual overall loss of skeletal muscle mass and muscle strength, and is closely associated with physical disability and death (3,4). However, there is currently no treatment for sarcopenia and its diagnosis is complex (5,6). A microRNA (miRNA/miR) is a non-coding RNA ~22 nucleotides long, which serves an important role in regulating mRNA expression at the post-transcriptional level by degrading and/or inhibiting the translation of mRNAs with sequences complementary to the miRNA (7-9). In most cases, primary miRNAs are transcribed from miRNA-encoding DNA, processed into precursor miRNAs, transported to the cytoplasm and then processed into miRNAs (10). Numerous studies have aimed to identify miRNAs that may serve as biomarkers or treatments of muscular diseases (11-13). However, the levels of precursor miRNAs do not exhibit clear positive correlations with those of mature miRNAs (14). A previous study demonstrated that the expression of miR-886 is increased in prostate cancer (15), whereas another study revealed that the expression of precursor miR-886 is decreased (16). These findings suggested that precursor miRNA levels may not be positively correlated with mature miRNAs, even during disease. The role of precursor miRNAs in muscle atrophy remains largely unknown, suggesting that the levels of mature miRNAs associated with various muscle diseases may differ from those of their precursors. Overexpression of PHD finger protein 20 (PHF20) has been shown to inhibit skeletal muscle differentiation in mice, and to reduce the expression of proteins that regulate myogenesis in such mice (17), indicating that PHF20 serves negative roles in myogenesis and injury-induced muscle regeneration *in vivo*. These findings suggested that the PHF20 transgenic (TG) mouse may serve as a useful animal model when studying muscle atrophy.

The present study comprehensively analyzed the miRNA precursor expression profiles in exosomes from human skeletal muscle. The findings revealed a previously unidentified muscle atrophy-associated miRNA precursor, the miR-206 precursor. Furthermore, miR-6516 was revealed to inhibit muscle atrophy. Notably, expression of the miR-206 precursor was upregulated during muscle atrophy, whereas miR-6516 was shown to serve a pivotal role in the regulation of muscle atrophy by modulating the expression of cyclin-dependent kinase inhibitor 1b (*Cdkn1b*).

Materials and methods

Plasma samples from patients and normal subjects. For experiments using human derivatives, materials, methods, ethical considerations and reasons for exemption from research subject consent were reviewed by the institutional review board of Chungnam National University Hospital, and exemption from review was approved on the condition that human derivatives were provided from a biobank (approval no. CNUH 2022-11-087; Daejeon, South Korea). All human plasma samples were provided by the biobank of Chungbuk National University Hospital. All human plasma samples were collected and stored in advance by the biobank with informed patient consent. Normal and patient plasma samples were obtained from individuals with disease codes Z00 (people without symptom complaints or reported diagnoses) and N18.5 (stage 5 chronic kidney disease), respectively, according to the Korean Standard Classification of Diseases (www.kcdcode.kr). The patient group was further adjusted to those with a history of diabetes. In addition, clinical information on the age, disease code, and additional diseases of the normal and patient groups was provided by the biobank. A total of 1 ml plasma was received from each of the 20 normal subjects (average age, 23.4 years; 10 men and 10 women) and 19 patients (average age, 64.8 years; 9 men and 10 women).

Animals. The Institutional Animal Care and Use Committee of Chungnam National University approved all animal management and experiment protocols (approval nos. 202305A-CNU-083 and 202309A-CNU-155; Daejeon, South Korea). All mice were bred and maintained in a controlled environment (free access to food and water, 12-h light/dark cycle, 50-60% humidity, 22°C ambient temperature). A total of 18 male C57BL/6 mice, 10 to 12 weeks old, were supplied by Narabiotech (Seoul, South Korea). A total of five 12-week-old male PHF20-overexpressing C57BL/6J mice that we had previously generated and maintained were used (17). At the end of the study, mice were euthanized by CO_2 gas inhalation at a CO_2 filling rate of 30% of the chamber volume/min. Before cardiac perfusion of all the mice, the mice were anesthetized with Avertin (200 mg/kg) and perfused first with PBS and then with 4% paraformaldehyde. To ensure sacrifice, euthanasia was performed using CO_2 at the aforementioned rate before specimen collection. The gastrocnemius, tibialis and soleus muscles of the mice were collected and used in the experiments. All mice experiments were conducted at animal facilities in accordance with institutional guidelines.

Cell-free (cf)RNA isolation from plasma. Human plasma stored at -80°C was rapidly thawed at room temperature, centrifuged at 4°C for 10 min at 2,000 x g, and the supernatant was transferred to a sterile 1.5-ml tube. Subsequently, 15 μl concentrated cfRNA was extracted using the Quick-cfRNA Serum & Plasma Kit (cat. no. 1059; Zymo Research Corp.) according to the manufacturer's instructions, and was immediately stored at -80°C.

RNA extraction from skeletal muscle. Blood effects were minimized through cardiac perfusion before muscle collection. The gastrocnemius, soleus and TA muscles located on the hind limb of the mice were collected, and any fat tissue was carefully removed without further injuring the muscle tissues. For cfRNA isolation, fresh skeletal muscle tissues were collected from mice and immediately placed in a 3.5-cm dish containing Dulbecco's Modified Eagle's Medium (cat. no. LM001-06; Welgene, Inc.) supplemented with 10% exosome-depleted FBS, 4 mM L-glutamine and 5.5 mM D-glucose. The tissues were incubated in a humidified incubator at 37°C and 5% CO_2 for 24 h, allowing them to release muscle-derived cfRNA under conditions resembling the natural environment within the body. Subsequently, 15 μl concentrated cfRNA was extracted using the Quick-cfRNA Serum & Plasma Kit, according to the manufacturer's instructions. In addition, total RNA was extracted from the gastrocnemius and TA muscles using TRIzol according to the manufacturer's protocol.

Reverse transcription-quantitative PCR (RT-qPCR). cDNA synthesis was performed using SuperScript™ II Reverse Transcriptase (cat. no. 18064022; Invitrogen; Thermo Fisher Scientific, Inc.) according to the manufacturer's instructions. For cDNA synthesis, 300 ng human plasma-derived cfRNA, 500 ng mouse gastrocnemius and tibialis muscle-derived cfRNA, 300 ng mouse soleus muscle-derived cfRNA, and 1 μg mouse gastrocnemius and tibialis anterior (TA) muscle-derived total RNA samples were used. cDNA was diluted 1:50 for qPCR on a Bio-Rad CFX96 Real-Time PCR Detection System (cat. no. 3600037; Bio-Rad Laboratories, Inc.) using GoTaq® qPCR Master Mix (cat. no. A6001; Promega Corporation). The expression levels of each mature mRNA and precursor of hsa-miRNA and mmu-miRNA were normalized to the expression levels of *Gapdh* for mature mRNAs, to *U6* for hsa-miRNA and to small nucleolar RNA (*snoRNA*)*202* for mmu-miRNAs. The qPCR thermal cycling conditions were as follows: Initial heat activation at 95°C for 2 min, followed by 40 cycles at 95°C for 15 sec and 60°C for 1 min. The Cq value was defined using Bio-Rad CFX Maestro 2.8 software (Bio-Rad Laboratories, Inc.). The relative RNA expression levels were quantified using the $2^{-\Delta\Delta Cq}$ method (ΔCq=Cq Target gene-Cq Normalization gene) (18). The primer sequences are listed in Table I.

Cell culture. Human skeletal muscle cells obtained at passage two (cat. no. CC-2561; Lonza Group, Ltd.) were cultured in SkBM Basal Medium (cat. no. CC-3161; Lonza Group, Ltd.) containing SkGM SingleQuots Supplements and Growth Factors (cat. no. CC-4139; Lonza Group, Ltd.). Exosome-depleted FBS (10%; cat. no. A2720801; Gibco; Thermo Fisher Scientific, Inc.) was added to the cell medium. The cells were cultured at 37°C in a humidified incubator containing 5% CO_2. Cells were subcultured at 80% confluence. Human skeletal muscle cells were differentiated when they reached 60% confluence for 5 days using Human Skeletal Muscle Cell Differentiation Medium (cat. no. 151D-250; Cell Applications, Inc.). The medium was changed every day during differentiation. The morphology of differentiated muscle cells was confirmed using an optical microscope. Cells were used for experiments for up to 5 passages. *Mycoplasma* negativity was confirmed before all cell experiments.

Western blot analysis. As described previously (19), after the completion of experiments for western blot analysis, cells

Table I. Primer sequences.

Gene symbol	Primer sequence (5'-3')
hsa-miR-12136	F: CCATGGGGTTGGCTTGAAAC
precursor	R: CAAAAAAGGAAGGAATCGAACCCC
hsa-miR-1291	F: TGTACTGTGGCTGTTGGTTTCA
precursor	R: CAGGAAGACAGTCCTTTAGGCCTC
hsa-miR-3651	F: GATTCGATGGGCCATAGCA
precursor	R: TGAGGAGAAGCAGCCTCC
hsa-miR-206	F: TTCCCGAGGCCACATGCTTC
precursor	R: CCATAGCAAAGTAATCCATATGGGG
hsa-miR-133b	F: CCTCAGAAGAAAGATGCCC
precursor	R: TCTCCAAGGACTGGGCAT
hsa-miR-664a	F: GAACATTGAAACTGGCTAGG
precursor	R: TTTTTCATTTTGTAGGCTGG
human U6	F: CTCGCTTCGGCAGCACA
	R: AACGCTTCACGAATTTGCGT
mmu-miR-206	F: CCAGGCCACATGCTT
precursor	R: TTCCATAGTGCTGAGATATC
mmu-miR-1291	F: AGAATCAAGGGATGGGAGGTTACC
precursor	R: GAAGACAGTTCTCTAGGCGTCTGC
mmu-miR-6516	F: AACCTCTTCCCTGGGGTTAG
precursor	R: CCACCAAACTGCTGCTAGG
mmu-miR-23a	F: GATTTGATGCCAGTCACA
precursor	R: GGGTCAGTTGGAAATCC
mmu-miR-664	F: TGACTGGATAGAAAACATTATTC
precursor	R: CTTTCATGTGTAGGCTGG
mouse	F: GCTGTACTGACTTGATGAAAGTAC
snoRNA202	R: CATCAGATGGAAAAGGGTTCAA
mouse Phf20	F: CATTGACTACGAAGAAGGGAG
	R: CTTCTCTAAAGGGCGCAGATA
mouse Trim63	F: GCTGGTGGAAAACATCATTGACAT
	R: CATCGGGTGGCTGCCTTT
mouse Cdkn1b	F: TCAAACGTGAGAGTGTCTAACGG
	R: AGGGGCTTATGATTCTGAAAGTCG
mouse Usp25	F: CAGAAGCACCAGCAGACATTT
	R: TGGCATTCTTTGCAGTGAGGA
mouse Pax7	F: GTGCCCTCAGTGAGTTCGATTAGC
	R: CCACATCTGAGCCCTCATCCA
mouse Myod1	F: CCACTCCGGGACATAGACTTG
	R: AAAAGCGCAGGTCTGGTGAG
mouse Gapdh	F: GACCCCTTCATTGACCTC
	R: GCCATCCACAGTCTTCTG

F, forward; miR, microRNA; R, reverse.

and muscles from mice were placed on ice and proteins were extracted using PRO-PREP™ Protein Extraction Solution (cat. no. 17081; Intron Biotechnology, Inc.). The lysates were then centrifuged for 30 min, 20,000 x g at 4˚C. The extracted proteins was quantified using the Bradford method and 25 µg protein was loaded per lane. Quantified proteins were separated by SDS-PAGE on 10.0% gels and were transferred to PVDF blotting membranes (cat. no. 10600023; Cytiva).

Subsequently, the transferred membranes were blocked in 1X Tris-buffered saline [140 mM NaCl, 2.7 mM KCl and 250 mM Tris-HCl (pH 7.4)] containing 5% skimmed milk and 0.2% Tween-20 for 1 h at room temperature. Blocked membranes were then incubated with primary antibodies (dilution ratio, 1:1,000) overnight at 4˚C, followed by incubation with secondary antibodies (dilution ratio, 1:10,000) for 1 h at room temperature. The following primary antibodies were used: Anti-MYOD (cat. no. sc-377460; Santa Cruz Biotechnology, Inc.), anti-PHF20 (cat. no. 3934S; Cell Signaling Technology, Inc.), anti-muscle RING-finger protein-1 (MuRF1; cat. no. sc-398608; Santa Cruz Biotechnology, Inc.), anti-tumor susceptibility gene 101 (TSG101; cat. no. sc-7964; Santa Cruz Biotechnology, Inc.), anti-calnexin (cat. no. 2679; Cell Signaling Technology, Inc.) and anti-GAPDH (cat. no. A19056; ABclonal Biotech Co., Ltd.). The following secondary antibodies were used: HRP-conjugated anti-rabbit (cat. no. 7074V; Cell Signaling Technology, Inc.) and HRP-conjugated anti-mouse (cat. no. 31430; Invitrogen; Thermo Fisher Scientific, Inc.). Protein expression was visualized using ProNA ECL (cat. no. TLP-112.1; TransLab, Co., Ltd.) according to the manufacturer's instructions. All protein expression levels were normalized to the expression levels of the loading control GAPDH. ImageJ software (version 1.49; National Institutes of Health) was used for semi-quantification of blotting.

Exosome isolation from conditioned media. Two 10-cm plates were used for exosome isolation. ExoQuick-TC™ (cat. no. EXOTC50A-1; System Biosciences, LLC) was used to isolate exosomes from the growth media, cultured for 24 h after media change, of pre-differentiation and post-differentiation skeletal muscle cells. Concentrated media (20 ml) were centrifuged at 3,000 x g for 15 min at room temperature to remove cells and cell debris. Subsequently, 4 ml ExoQuick-TC was added to the supernatant. After inverting at least five times, the samples were incubated at 4˚C overnight (≥12 h), then centrifuged at 1,500 x g for 30 min at room temperature. The supernatant was discarded and the pellet was resuspended in TRIzol® (cat. no. 15596026; Invitrogen; Thermo Fisher Scientific, Inc.) for precursor miRNA profile analysis. After resuspending the exosomes in TRIzol, they were immediately stored at -80˚C before starting precursor miRNA profiling analysis.

Precursor miRNA profile analysis. The miRNeasy® Serum/Plasma Kit (cat. no. 217184; Qiazen, Inc.) was used to prepare RNA samples. The RNA isolated from each sample was used to construct sequencing libraries with the SMARTer smRNA-Seq Kit for Illumina (Takara Bio, Inc.), following the manufacturer's protocol. Briefly, input RNA was first polyadenylated in order to provide a priming sequence for an oligo-(dT) primer. cDNA synthesis was primed by the 3' smRNA dT Primer, which incorporated an adapter sequence at the 5' end of each first-strand cDNA molecule. When the MMLV-derived PrimeScript™ Reverse Transcriptase (cat. no. 2680A; Takara Bio Inc.) reached the 5' end of each RNA template, it added non-templated nucleotides, which are bound by the SMART smRNA Oligo-enhanced with locked nucleic acid (LNA) technology for greater sensitivity. In the template-switching step, PrimeScript RT used the SMART smRNA Oligo as a

template for the addition of a second adapter sequence to the 3' end of each first-strand cDNA molecule. In the next step, full-length Illumina adapters (including index sequences for sample multiplexing) were added during PCR amplification. The Forward PCR Primer bound to the sequence added by the SMART smRNA Oligo, while the Reverse PCR Primer bound to the sequence added by the 3' smRNA dT Primer. Resulting library cDNA molecules included sequences required for clustering on an Illumina flow cell. The libraries were validated by checking the size, purity and concentration on the Agilent Bioanalyzer. The libraries were pooled in equimolar amounts, and sequenced on an Illumina HiSeq 2500 instrument. Image decomposition and quality values calculation were performed using the modules of the Illumina pipeline All exosomal precursors of miRNA sequencing procedures were performed by Macrogen, Inc. Sequence alignment and detection of known and novel precursors of miRNA were performed using the miRDeep2 software algorithm (Ver. 2.0.0.8; Max Delbrück Center). In the read alignment to precursor result of the Quantifier module result of miRDeep2, the read aligned to each precursor was selected. Among the selected reads, reads that were assigned to mature miRNA were excluded, and reads with a length of >50% of the precursor were selected. Reads per million (RPM) was calculated using the total sum of reads for each sample obtained from the selected results. All exosomal precursors of miRNA sequencing procedures were performed by Macrogen, Inc. From the analysis results of precursor miRNA sequencing, as a cutoff point, abundant precursor miRNAs >700 RPM were selected as biomarker candidates.

Grip strength test. To measure hindlimb grip strength, mice at 12 weeks old were placed on a grip strength meter, while their tail and nape were held and pulled gently. Each mouse was allowed to perform the test five times and was given a 5-min break between each test. Values for grip strength were recorded and normalized by dividing by whole body weight.

RNA correlation analysis. To evaluate the relationship between the expression of genes in skeletal muscle, Gene Expression Profiling Interactive Analysis 2 (GEPIA2) (http://GEPIA2.cancer-pku.cn/index.html) (20) was used, and a Spearman correlation analysis was performed. Only human skeletal muscle tissue databases (n=396) from GTEx (21) were used for the analysis.

Histological analysis of muscle tissue. Gastrocnemius and tibialis muscle tissues from mice were fixed with 4% paraformaldehyde for 16 h at 4°C and 4-μm paraffin-embedded sections were generated. The paraffin-embedded sections were stained with hematoxylin (for 5 min at room temperature) and eosin (for 1 min at room temperature) according to standard protocols. Light microscopy was used for histological observation. Measurements of cross-sectional area (CSA) were performed using ImageJ software (version 1.49; National Institutes of Health). For each CSA, six different views were randomly selected for measurement.

Immobilization model. The right hind limbs of 13 10-week-old male C57BL/6 mice supplied by Narabiotech (Seoul, South Korea) were used. As described in a previous study, surgical tape was wrapped around starting from the distal aspect of the foot to the ankle area. Subsequently, Velcro was wrapped around the hindlimb, starting at the distal end of the foot. Velcro was replaced if adverse effects (e.g., skin injury and edema) or loose Velcro was observed. The forepaw and left hindlimb were free, so that the mice had free access to food and water.

Bioinformatic analysis. Using Human TargetScan (Ver 8.0; https://www.targetscan.org/vert_80/) and mouse TargetScan (Ver 8.0; https://www.targetscan.org/mmu_80/), target mRNAs for microRNAs were scrutinized.

Muscle injury and administration of miRNA. To transfer miR-6516 to TA muscles of immobilization-injured mice, mimic-miR-6516 (cat. no. SMM-003; 20 nM; Bioneer Corporation) was mixed with RNAiMAX (cat. no. 13778030, Invitrogen; Thermo Fisher Scientific, Inc.), as described previously (22). For the control group, mimic-miR-control (cat. no. SMC-2003; Bioneer Corporation) was used and a mixture was prepared in the same manner as the mimic-miR-6516 mixture. The resulting mixture (50 μl) was injected on the 5th and 10th day during the 14-day immobilization period, and the Velcro was replaced after injection.

Statistical analysis. Data are expressed as the mean and standard error of the mean (SEM) from at least three separate experiments. GraphPad Prism (version 8.1.1; Dotmatics) was used for statistical analysis. Quantitative data are presented as the mean ± SEM unless indicated otherwise. Comparisons between two groups were evaluated using unpaired Student's t-test or Mann-Whitney U test, depending on the results of the Shapiro-Wilk test. For multiple comparisons, one-way ANOVA was performed, followed by Dunnett's post hoc test. P<0.05 was considered to indicate a statistically significant difference.

Results

Circulating precursors of miR-206 and miR-664a increase on development of sarcopenia-related disease. It has previously been shown that miRNA expression levels are not always proportional to those of precursor miRNAs (14), suggesting that the changes in miRNA levels observed as muscular atrophy develops may differ from the changes in precursor miRNA levels. To profile the skeletal muscle-derived miRNA precursors secreted into the plasma (possible biomarkers of muscle atrophy), the exosomal miRNA precursors (cfRNAs) of human muscle cells were first sequenced. Muscle cell differentiation was confirmed by the gross changes in fused cell morphology and increased expression of MYOD (Fig. 1A and B). Exosomes were extracted using ExoQuick, and western blotting detected the positive exosomal marker TSG101 but not the negative marker calnexin (Fig. 1C). Exosomal precursor miRNA sequencing results confirmed that precursor miRNAs were abundant in exosomes derived from pre- and post-differentiated muscle cells (Table II). Of such precursor miRNAs, any that overlapped with other genes or were difficult to analyze via qPCR were excluded.

Table II. Abundant pre-miRNAs in exosomes derived from human skeletal muscle cells.

Precursor miRNA	Reads per million	
	Pre-differentiated	Differentiated
miR-12136	6.7×10^5	1.18×10^5
miR-1291	6.72×10^3	7.97×10^2
miR-23a	8.52×10^2	5.31×10^2
miR-3651	2.7×10^3	8.4×10^4
miR-4449	4.83×10^3	1.75×10^4
miR-6516	2.79×10^3	1.38×10^4
miR-664a	1.04×10^3	-
miR-664b	7.1×10^2	-
let-7a-3	1.89×10^2	7.97×10^2
miR-10394	9.47×10^1	7.97×10^2

miR/miRNA, microRNA.

The precursor of miR-206, known to be a muscle-only miRNA (23), and the precursor of miR-133b, which is downregulated in the plasma of patients with sarcopenia (24), were analyzed in the present study. Previous studies have shown that some snoRNAs also function as precursors of miRNAs (25-28). Precursors of miRNAs that overlapped with snoRNAs that were not identified as producing miRNAs were excluded from the analysis, even if they did not overlap in sequence with a specific mRNA. Another study reported that miR-1291 and miR-3651 are derived from snoRA2C and snoRD84, respectively, and these snoRNAs are very similar in terms of their sequences to the precursors of the corresponding miRNAs (29). For this reason, the precursors of miR-1291 and miR-3651 were not excluded from the analysis, despite their significant sequence overlap with snoRA2C and snoRD84. In addition, the precursor of miR-4449 was excluded from the analysis, as primer design and RT-qPCR were difficult to perform given the 86% G+C content. In summary, in human plasma-derived cfRNAs, the precursors of miR-206, miR-12136, miR-1291, miR-664a, miR-3651 and miR-133b were selected for analysis. Given the low number of patients diagnosed with sarcopenia, patients with diseases likely to cause sarcopenia as a complication were included. Previous studies have revealed that the incidence of sarcopenia is high in patients with diabetes and chronic kidney disease (30,31). Therefore, the biomarker candidates were quantitatively analyzed in the plasma of patients with either of these diseases, and of normal people aged 20-30 years. Of the biomarker candidates, the expression levels of precursors of miR-206 and miR-664a were significantly increased in the patient group with diabetes and chronic kidney disease (Fig. 1D). By contrast, there were no significant differences in the expression levels of the precursors of miR-133b, miR-1291, miR-3651 and miR-12136 between patients and control individuals (Fig. 1E). These results suggested that increased expression of the precursors of miR-206 and miR-664a in circulating plasma cfRNAs may be associated with sarcopenia, which is characterized by muscle atrophy.

PHF20 overexpression induces muscular atrophy in vivo. The patients analyzed in the present study were expected to develop muscle atrophy as a complication of diabetes or chronic kidney disease; however, atrophy was not definitively confirmed. Therefore, the present study analyzed muscle-derived cfRNAs in a mouse model of muscular atrophy. Induction of atrophy was confirmed in mice overexpressing PHF20. In a previous study, PHF20 exerted a negative effect on muscle differentiation via positive regulation of YY1 (17). Subsequently, correlations between PHF20 levels and those of gene products associated with muscle differentiation, namely MYH2, TNNT1 and TNNT3, were assessed (32). The relationships between the levels of the muscle atrophy markers MuRF1 (*TRIM63*) and atrogin-1 (*FBXO32*), and their upstream transcription factor FOXO3a (33,34), were also investigated. These studies confirmed the negative association between the levels of PHF20 and those of muscle differentiation genes, and the positive association between the levels of PHF20 and muscle atrophy genes. The correlation pattern between PHF20 and each marker gene was similar to the correlation pattern between YY1 and each marker gene (Fig. 2A). The correlation of genes was analyzed using the dataset from GTEx. These findings indicated the possibility that PHF20 overexpression may inhibit muscle differentiation and facilitate muscle atrophy. A previous study confirmed that overexpression of PHF20 inhibits muscle differentiation and triggers defects in muscle morphology *in vivo* (17). This suggests that overexpression of PHF20 may induce muscle atrophy; additional experiments were thus performed in the present study to assess this. In PHF20 TG mice, the expression levels of both PHF20 and the muscle atrophy marker MuRF1 were increased (Fig. 2B), as were the mRNA expression levels of *Phf20* and *Trim63*, which encode PHF20 and MuRF1 (Fig. 2C). The grip strength test was used to evaluate the muscle strength of PHF20 TG mice (35), and the strength was significantly lower than that of wild-type mice (Fig. 2D). Additionally, the muscle CSA was significantly reduced in PHF20 TG mice compared with that in wild-type mice (Fig. 2E). These results provided clear evidence that overexpression of PHF20 induced muscular atrophy *in vivo*.

Muscle immobilization induces muscle atrophy and secretion of atrophied muscle-derived cfRNAs. Muscle atrophy attributable to muscle disuse is a common clinical problem and one of the major causes of muscle atrophy (36,37). Therefore, to identify candidate biomarkers of muscle atrophy not only in the PHF20-overexpressing mouse model but also in a mouse model of muscle atrophy induced by muscle disuse (immobilization), muscle atrophy was induced in wild-type mice via Velcro immobilization. In previous studies, it was confirmed that muscle atrophy was induced when the hind limb was immobilized using Velcro for 2 weeks (38,39). Therefore, the right hind limbs of 10-week-old male wild-type mice were immobilized for 2 weeks to induce muscle atrophy (Fig. 3A). Notably, the muscle CSA level of the hind leg that was fixed with Velcro was decreased compared with that in non-treated wild type mice (Fig. 3B). Skeletal muscle atrophy causes biochemical and physiological changes in the muscles, leading to alterations in gene expression (40). These characteristics suggest that atrophied muscles in PHF20-overexpressing mice
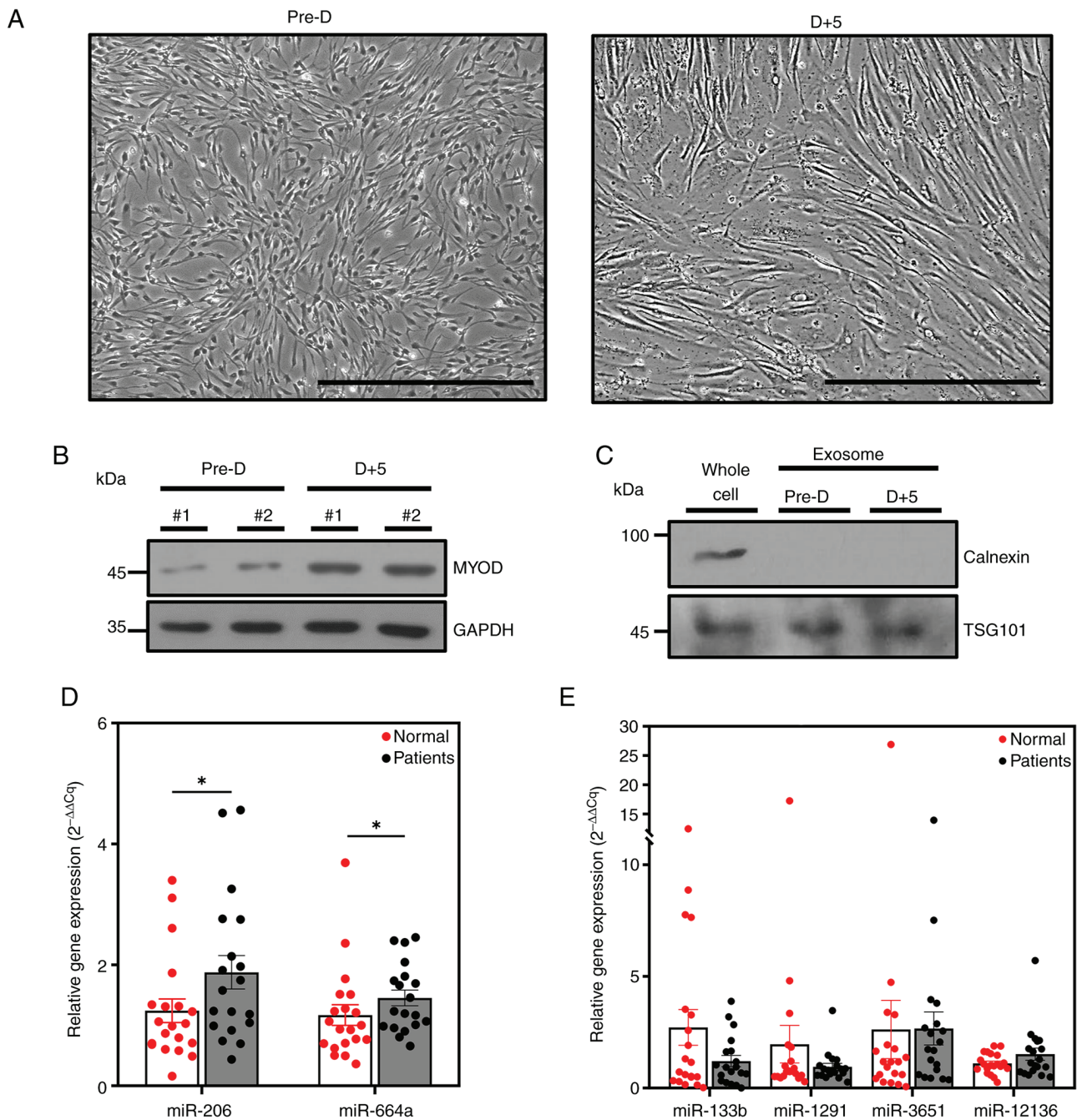
Figure 1. Changes in the expression levels of precursors of miRNA in patients at risk of sarcopenia compared with healthy subjects. (A) Optical micrographs of human skeletal muscle cells before differentiation (left image) and after differentiation (right image). Scale bars, 500 μm. Changes in the protein expression levels of (B) MYOD, and (C) TSG101 and calnexin were analyzed by western blotting using the corresponding antibodies. (D) Expression levels of precursors of miR-206 and miR-664a were significantly different in patients (n=19) compared with in normal subjects (n=20). (E) Expression levels of precursors of miR-133b, miR-1291, miR-3651 and miR-12136 were not significantly different in patients (n=19) compared with in normal subjects (n=20). Expression levels of miRNA precursors were normalized to *U6* expression levels. Data are presented as the mean ± SEM. *P<0.05. Pre-D, pre-differentiation; D+5, differentiated day 5; miRNA/miR, microRNA.

and Velcro-fixed mice may synthesize cfRNAs, the levels of which may differ from those of non-fixed wild-type mice; therefore, further analysis of muscle atrophy biomarker candidates was performed to identify changes in expression levels.

Muscle atrophy affects the expression levels of multiple miRNA precursors in skeletal muscle. As aforementioned, to obtain cfRNAs from atrophied muscles, the right hind limbs of five 10-week-old male wild-type mice were fixed with

Velcro for 2 weeks to induce muscle atrophy; subsequently, the gastrocnemius, soleus and TA muscles were dissected, and cfRNAs were extracted from each muscle. Similarly, the gastrocnemius, soleus and TA muscles of 12-week-old male PHF20 TG mice were prepared, and cfRNAs were extracted from each muscle. For the same reasons presented when selecting precursor miRNAs to be analyzed in human plasma, the precursors of miR-206, miR-6516, miR-1291, miR-23a and miR-664 were selected for mouse analysis. In
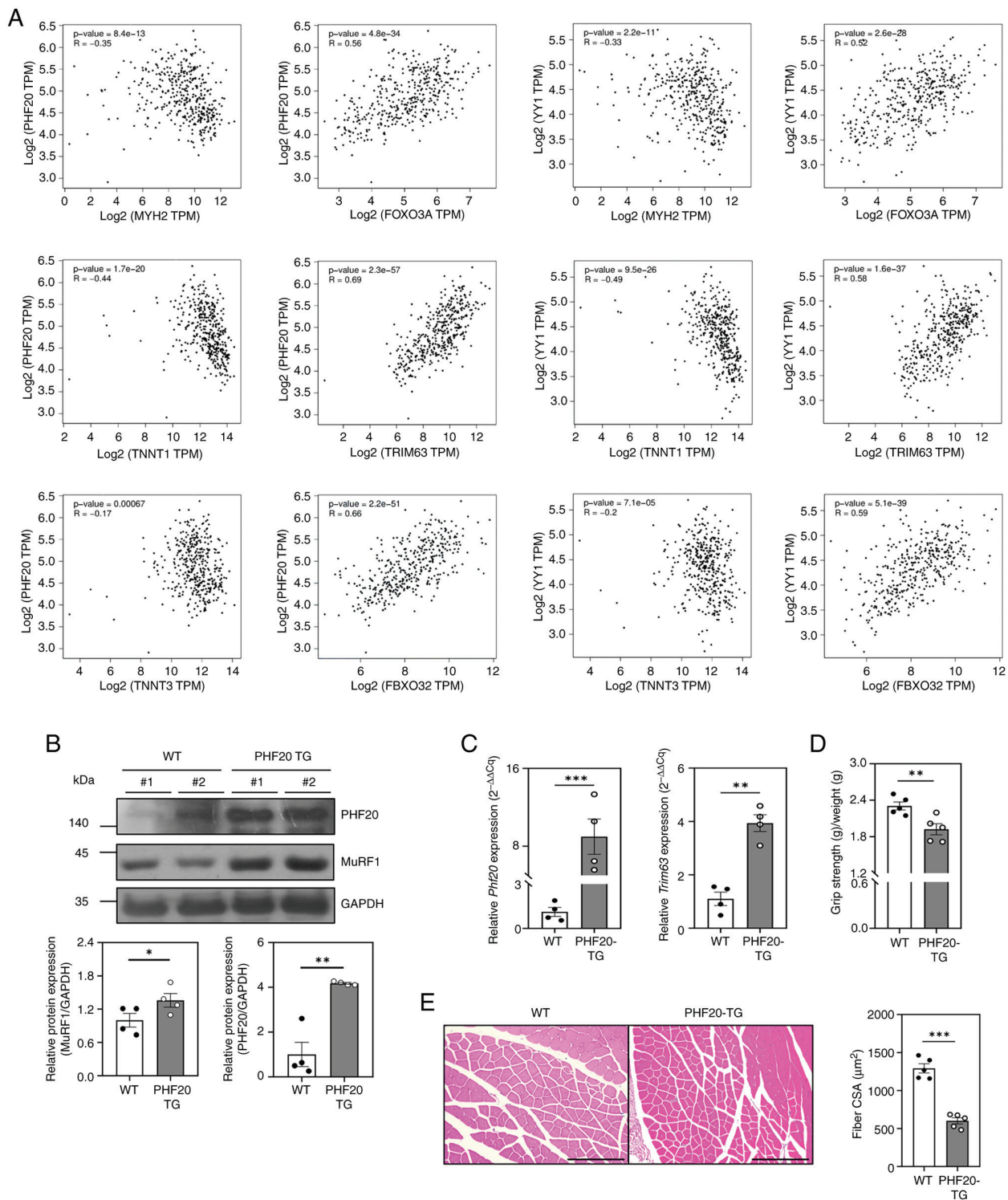
Figure 2. Effect of PHF20 overexpression on muscles *in vivo*. (A) Correlation of gene pairs in skeletal muscle samples (n=396) present in the GTEx database. Correlation analysis of PHF20 and YY1 with muscle differentiation marker genes MYH2, TNNT1 and TNNT3, and muscle atrophy marker genes FOXO3A, TRIM63 and FBXO32. (B) Lysates were extracted from gastrocnemius muscle tissues from WT (n=4) and PHF20-TG mice (n=4). Changes in protein expression levels were analyzed by western blotting with the corresponding antibodies. (C) Total RNA was extracted from gastrocnemius muscle tissues from 12-week-old male WT (n=4) and PHF20-TG mice (n=4). Expression levels of *Phf20* and *Trim63* were analyzed by reverse transcription-quantitative PCR. Expression levels were normalized to *Gapdh*. (D) Hindlimb grip strength test of 12-week-old male WT (n=5) and PHF20 TG (n=5) mice. (E) Gastrocnemius muscle cross sections of 12-week-old male WT (n=5) and PHF20-TG (n=5) mice stained with hematoxylin and eosin. Each CSA was measured with ImageJ software, and six different views were randomly selected for CSA measurement. Scale bars, 200 μm. Data are presented as the mean ± SEM. *P<0.05, **P<0.01, ***P<0.001. CSA, cross-sectional area; MuRF1, muscle RING-finger protein-1; PHF20, PHD finger protein 20; TG, transgenic; WT, wild-type.

mice, miR-664 is not divided into miR-664a and miR-664b; therefore, the precursor of miR-664 was included in the analysis. In the immobilized mice, the expression levels of the precursor of miR-206 were increased in cfRNAs derived from the gastrocnemius, soleus and TA muscles compared with wild type mice; also the expression levels of the
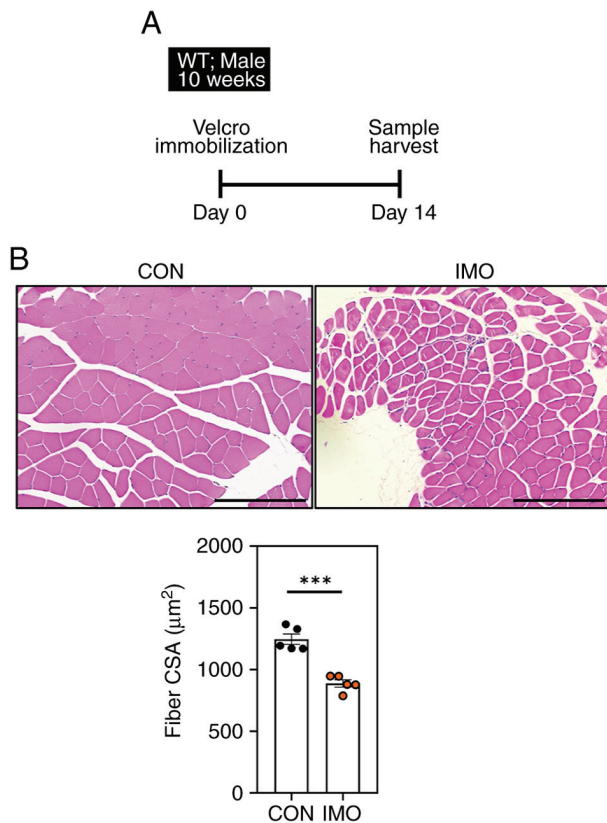
Figure 3. IMO-injury model with induced muscle atrophy. (A) Schematic diagram of the experimental procedures. The right hind legs of 10-week-old male WT mice were fixed using Velcro for 2 weeks and then samples were harvested. (B) CSA measured after IMO injury. Gastrocnemius muscle cross sections of 12-week-old male CON (n=5) and Velcro-immobilized (n=5) mice were stained with hematoxylin and eosin. Each CSA was measured with ImageJ software and six different views were randomly selected for CSA measurement. Scale bars, 200 μm. Data are presented as the mean ± SEM. ***P<0.001. CON, control; CSA, cross-sectional area; IMO, immobilization; WT, wild-type.
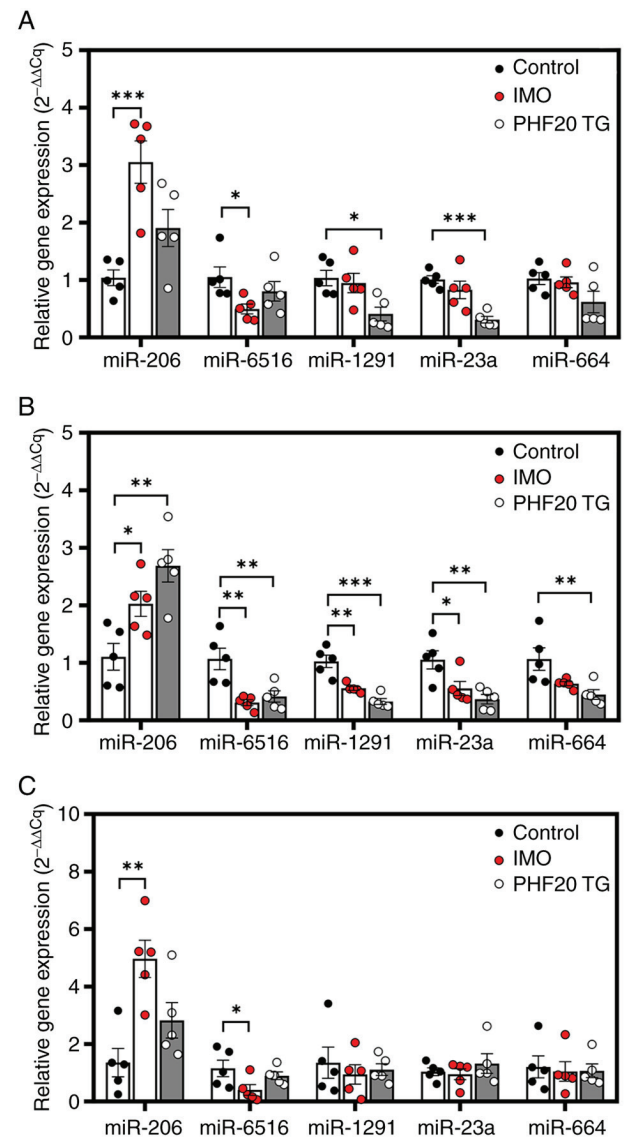

Figure 4. Expression of miRNA precursors in mice with IMO-induced muscle atrophy or in PHF20 TG mice with muscle atrophy. Expression levels of miRNA precursors in cell-free RNA samples derived from (A) gastrocnemius, (B) TA and (C) soleus muscles in WT (control), IMO and PHF20-TG mice (n=5/group). Expression levels were normalized to small nucleolar RNA 202 expression levels. Data are presented as the mean ± SEM. *P<0.05, **P<0.01, ***P<0.001. IMO, immobilization; miR/miRNA, microRNA; PHF20, PHD finger protein 20; TA, tibialis anterior; TG, transgenic; WT, wild-type.

precursor of miR-6516 were decreased (Fig. 4A-C). In addition, the expression levels of the precursors of miR-1291 and miR-23a were decreased in the TA muscle-derived cfRNAs from immobilized-mice compared with those from wild-type mice (Fig. 4B). In the PHF20 TG mice, the expression levels of the precursor of miR-206 were increased in cfRNAs derived from the TA muscles compared with those from wild-type mice (Fig. 4B); also the levels of the precursor of miR-6516 decreased (Fig. 4B). In addition, the expression levels of the precursors of miR-1291 and miR-23a were decreased in gastrocnemius muscle-derived cfRNAs from PHF20 TG mice compared with those in wild-type mice (Fig. 4A). The expression levels of the precursors of miR-1291, miR-23a and miR-664 were also decreased in the TA muscles of PHF20 TG mice compared with those in wild-type mice (Fig. 4B). It has previously been reported that miR-206 is a skeletal muscle-specific miRNA (23). Thus, as a mature miRNA is cleaved from a precursor of that miRNA, the precursor of miR-206 is also muscle-specific. Taken together, these experiments indicated that the expression levels of the precursor of miR-206 may increase in mouse muscle-derived cfRNAs during muscle atrophy and in plasma cfRNAs obtained from patients at risk of sarcopenia.

miR-6516 inhibits immobilization-induced muscle atrophy by regulating Cdkn1b. Notably, a decrease in the expression levels of the miR-6516 precursor was observed in all muscle-derived cfRNAs of Velcro-immobilized mice with muscle disuse atrophy. Based on these results, additional experiments were performed to determine whether miR-6516 administration in muscles affected muscle disuse-induced atrophy. During the 14-day period of muscle atrophy induced via Velcro immobilization of the right hind limb, a mimic-miR-6516 was injected into the TA muscle on days 5 and 10, and the mice were sacrificed on day 14 (Fig. 5A). It was confirmed that the muscle CSA of the mice administered mimic-miR-6516 was significantly greater than that of mice administered the mimic-miR-control, indicating that miR-6516 inhibits the progression of muscle
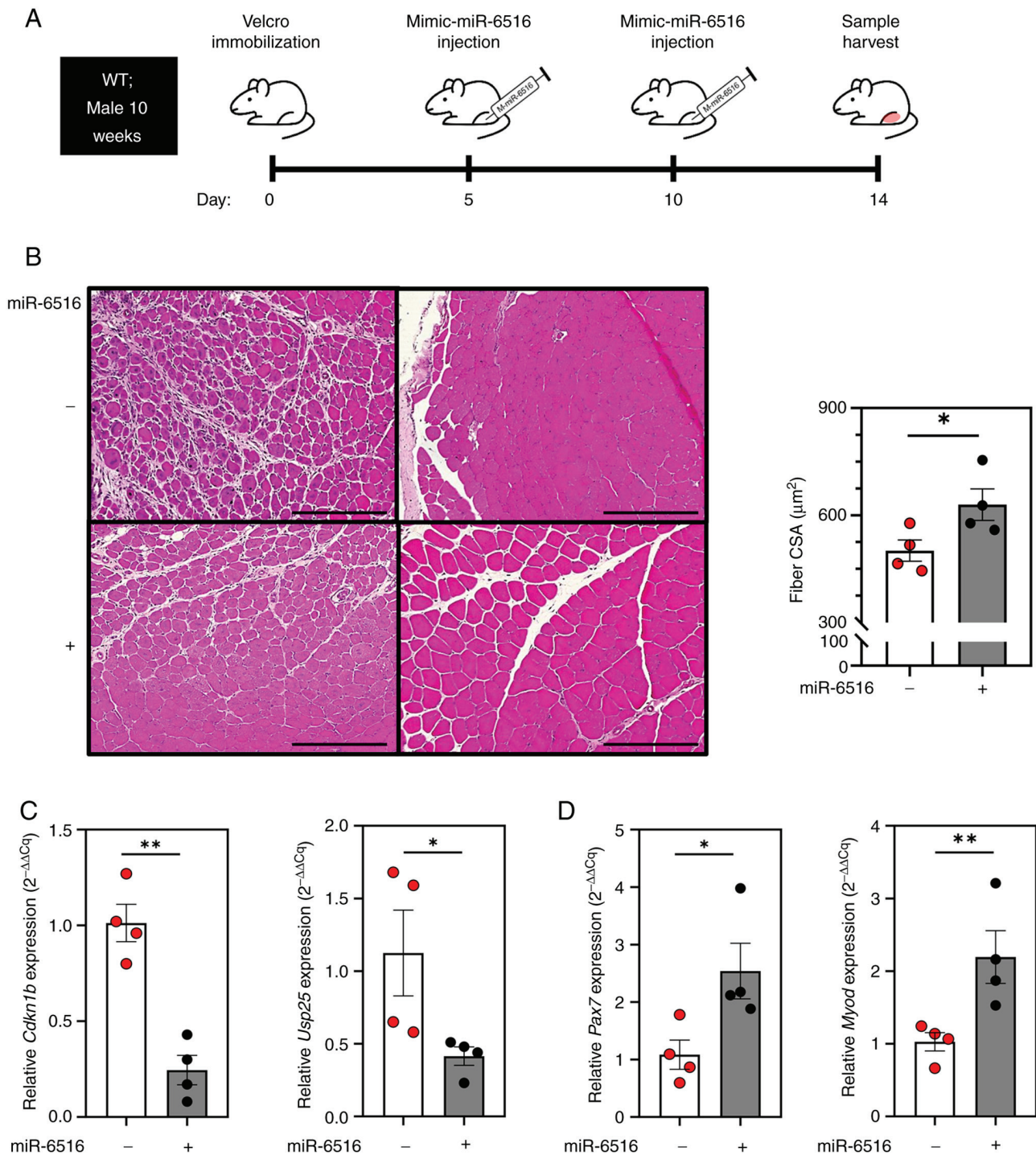
Figure 5. Effect of miR-6516 on suppressing muscle atrophy *in vivo*. (A) Schematic diagram of the experimental procedures. On days 5 and 10 of the 14-day immobilization-injury period of 10-week-old male WT mice, mimic-miR-6516 and control miRNA mimics were injected into the TA muscle of the right hind limb. (B) TA muscle cross sections of 12-week-old male mice injected with mimic-miR-control (n=4) and mimic-miR-6516 (n=4) stained with hematoxylin and eosin. Scale bars, 200 μm. Each CSA was measured with ImageJ software and six different views were randomly selected for CSA measurement. (C and D) Total RNA was extracted from TA muscle tissues from 12-week-old male mice injected with mimic-miR-control (n=4) and mimic-miR-6516 (n=4) during 14 days immobilization. Expression levels of (C) *Cdkn1b* and *Usp25*; (D) *Pax7* and *Myod1* were analyzed by reverse transcription-quantitative PCR. Expression levels were normalized to *Gapdh* expression level. Data are presented as the mean ± SEM. *$P<0.05$, **$P<0.01$. *Cdkn1b*, cyclin-dependent kinase inhibitor 1b; miR, microRNA; TA, tibialis anterior; *Usp25*, ubiquitin specific peptidase 25; WT, wild-type.

atrophy caused by muscle disuse (Fig. 5B). The genes targeted by miR-6516 when inhibiting muscle atrophy were subsequently investigated. Using TargetScan human (Ver. 8.0) and TargetScan mouse (Ver. 8.0), genes that were predicted to be common targets of miR-6516-3p or -5p in humans and mice

were identified, according to a cumulative weight context score of ≤-0.4. Additionally, since muscle atrophy was suppressed upon injection of mimic-miR-6516, only genes positively correlated with the muscle atrophy markers MuRF1 (*TRIM63*), Atrogin1 (*FBXO32*) and FOXO3a (*FOXO3a*) were selected as

Table III. CWCS of miR-6516 predicted target genes.

Predicted target gene symbol	hsa-miR-6516		mmu-miR-6516		Correlation with muscle atrophy genes
	-3p	-5p	-3p	-5p	
NPPC	-0.57	-	-0.49	-	Negative
CDKN1B	-0.47	-	-0.40	-	Positive
PRND	-	-0.48	-	-0.53	Negative
USP25	-	-0.46	-	-0.80	Positive

CDKN1B, cyclin-dependent kinase inhibitor 1b; CWCS, cumulative weighted context score; miR, microRNA; *NPPC*, natriuretic peptide C; *PRND*, prion like protein doppel; *USP25*, ubiquitin specific peptidase 25.
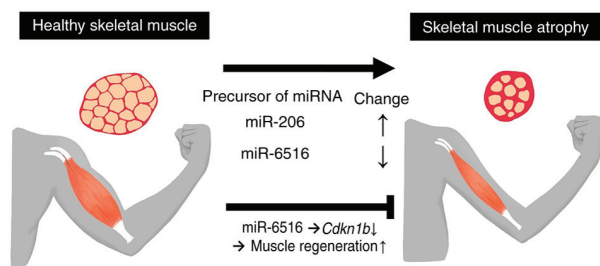

Figure 6. Summary figure. When muscle atrophy is induced in muscle by overexpression of PHF20 or other causes, expression of the precursors of miR-206 and miR-6516 increases. Additionally, during muscle atrophy caused by muscle disuse, treatment with miR-6516 can suppress the expression of *Cdkn1b*, thereby upregulating muscle regeneration and suppressing muscle atrophy. *Cdkn1b*, cyclin-dependent kinase inhibitor 1b; miR/miRNA, microRNA; PHF20, PHD finger protein 20.

possible target genes. Only *CDKN1B* (p27^{kip1}) and ubiquitin specific peptidase 25 (*USP25*; USP25) satisfied the aforementioned conditions, and they were predicted to be target genes of miR-6516 in the context of inhibition of muscle atrophy (Table III). The mimic-miR-6516 was injected to determine whether this affected the expression levels of *Usp25* and *Cdkn1b*. In mice injected with mimic-miR-6516, the expression levels of *Cdkn1b* and *Usp25* were significantly reduced (Fig. 5C). A previous study showed that p27^{kip1} levels negatively regulate skeletal muscle satellite cell proliferation and muscle regeneration (41). Additionally, a decrease in muscle fiber diameter has been confirmed in mice overexpressing *Cdkn1b* (42). As expected, the expression of early muscle regeneration markers *Pax7* and *Myod1* was increased in muscles administered mimic-miR-6516 (Fig. 5D). However, additional investigations are required because no association between suppression of muscle atrophy and reduction of *USP25* expression was conclusively shown (data not shown). Taken together, these data suggested that injection of mimic-miR-6516 during immobilization inhibits muscle rest-induced muscle atrophy by suppressing expression of *Cdkn1b* and promoting skeletal muscle satellite cell proliferation and muscle regeneration (Fig. 6).

Discussion

In the present study, precursor miRNAs from skeletal muscle cell-derived exosomes were sequenced in the search for biomarker candidates. Among the precursor miRNAs, those that were abundant were selected as possible candidates. In detail, precursor miRNAs with sequences that did not overlap with any mRNAs in humans and mice were selected. Candidate biomarkers were compared between plasma-derived cfRNAs from patients at a risk of sarcopenia and normal subjects. In addition, mouse muscle atrophy was confirmed after muscle immobilization injury and in PHF20 TG mice, and muscle-derived cfRNAs were compared with wild-type cfRNAs. Notably, both plasma-derived cfRNAs from patients and muscle-derived cfRNAs from mice with muscle atrophy due to disuse exhibited increased expression levels of the precursor of miR-206. Additionally, the expression levels of the precursor of miRNA-6516 were decreased in muscle-derived cfRNAs from mice subjected to muscle immobilization injury. When mimic-miR-6516 was injected into the TA muscle of such mice, the muscle immobilization-induced muscle atrophy caused by muscle disuse was suppressed via inhibition of *Cdkn1b*. Taken together, these findings indicated that the precursor of miR-206 was increased in plasma and muscle-derived cfRNAs during muscle atrophy, and that miR-6516 inhibited muscle rest-induced muscle atrophy, indicating the potential use of these miRNA precursors for diagnostic and therapeutic purposes.

In previous studies, miR-1, miR-133a, miR-133b and miR-206 have been reported to be myomiRs, i.e., miRNAs that are highly expressed specifically in muscle (43-46). In particular, miR-206 exhibits muscle-specific expression characteristics (43,45,47), and miR-133b is downregulated in the plasma of patients with sarcopenia (24). A previous study showed that the expression levels of mature miRNAs and their precursors are not positively correlated (14). However, studies on the precursors of miRNAs associated with muscle atrophy are lacking; therefore, miRNA precursors associated with muscle atrophy were targeted in the present study. Cell-derived miRNA precursors were investigated in the exosomes of human muscle cells, which also contained the precursors of muscle-specific miR-206 and sarcopenia-related miR-133b. It has previously been reported that increased p27^{kip1} expression in skeletal muscle inhibits muscle satellite cell capacity and proliferation, thereby compromising muscle regeneration (41). The results of the present study confirmed that the precursor of miR-6516 was reduced when muscle immobilization triggered atrophy, and that treatment of muscles with miR-6516

suppressed atrophy by inhibiting the expression of *Cdkn1b*. In addition, the precursor of miR-206 was confirmed to be upregulated in skeletal muscle-derived cfRNAs from mice with muscle atrophy due to disuse and in plasma-derived cfRNAs from patients at risk of sarcopenia. The present study thus suggested that the precursor of miR-206 may be considered a novel biomarker of muscle atrophy and that miR-6516 could inhibit muscle atrophy by reducing the expression of *Cdkn1b* in skeletal muscle. Expression of *Usp25*, another target mRNA of miR-6516, was also reduced by administration of mimic-miR-6516. However, to the best of our knowledge, how reduced *Usp25* expression might prevent muscle atrophy has not yet been investigated and further research is necessary.

Muscle wastes for a variety of reasons, including metabolic problems and muscle disuse (48-51), and it is regenerated from muscle progenitor cells (8,52,53). Overexpression of PHF20 in muscle inhibits the differentiation of muscle cells and thus suppresses muscle regeneration, disrupting the balance between muscle wasting and regeneration (17). In addition, muscle immobilization injury increases muscle wasting because of muscle disuse, also disrupting the balance between muscle wasting and regeneration (51,54-56). The present results revealed that the precursor of miR-206 was increased in all muscles of immobilization-injured mice and in the TA muscle of PHF20-overexpressing mice, whereas miR-6516 was generally decreased only in the muscles of the immobilization-injured group. These findings suggested that the change in the expression levels of the precursor of miR-206 may be in response to muscle loss, and that the change in the expression levels of the precursor of miR-6516 may be in response to the muscle atrophy caused by muscle disuse. The expression levels of the precursors miR-206 and miR-6516 were decreased in muscle atrophy-derived cfRNA. Although miR-206 is a well-known muscle-derived miRNA, there is a lack of research on the association between miR-6516 and skeletal muscle. Similarly, there is a lack of research on the association between miR-206 and miR-6516. Notably, the expression levels of the miR-206 and miR-6516 precursors were both decreased during skeletal muscle atrophy, indicating a significant relationship between the expression levels of precursors and muscle mass maintenance, which warrants further studies.

Previous studies have reported that miR-664a-5p is increased in circulating exosomes from patients with obesity and type 2 diabetes (57). The present study confirmed that the expression levels of the precursor of miR-664a were increased in the plasma of patients at risk of sarcopenia, suggesting that this may be caused by diabetes, which was common in the patient group.

The present study also revealed that the precursors of miR-1291, miR-23a and miR-664 were downregulated in the TA muscles of mice with confirmed muscle atrophy. The TA muscle is composed principally of fast-twitch muscles (58,59), suggesting that the precursors of miR-1291, miR-23a and miR-664 function as biomarkers of fast-twitch muscle atrophy. However, as these three miRNA precursors are produced in tissues other than skeletal muscle, fast-twitch muscle atrophy cannot be controlled only by the levels of skeletal muscle-derived miRNA precursors.

It may be beneficial to measure mature miRNAs in relation to precursor miRNAs in human plasma; however, due to the limited amount of plasma samples available, only quantitative analysis of miRNA precursors could be performed in the present study. The mature form of general precursor miRNA, which did not exhibit significant differences between the normal and patient groups, requires further research as it may be discovered as a new biomarker. Furthermore, due to the limited amount of muscle-derived cfRNA samples, the present study was unable to conduct quantitative analysis on targets other than miRNA precursors. It may also be advantageous to measure not only miRNA precursors, but also mature miRNAs and the proteins/mRNAs involved in their production. In addition, the relationship between miR-6516 and *Cdkn1b* expression needs to be confirmed. However, for reasons, such as those aforementioned, the effect of mimic-miR-6516 administration was confirmed, but it was not confirmed whether the expression levels of *Cdkn1b* were dependent on the expression levels of miR-6516; therefore, further research on this is necessary.

In conclusion, the present study provides evidence that the expression of the muscle-derived miR-206 precursor may be increased during muscle atrophy, supporting a role for this molecule as a muscle atrophy biomarker. Additionally, the present study provides evidence that miR-6516 administration to muscles could inhibit muscle rest-induced atrophy by suppressing *Cdkn1b*. Taken together, these results indicated that the miR-206 precursor may serve as a biomarker of muscle atrophy, and miR-6516 may serve as a candidate therapeutic target to inhibit muscle atrophy.

Availability of data and materials

The data generated in the present study may be found in the NCBI Sequence Read Archive under accession number PRJNA1088925 or at the following URL: https://www.ncbi.nlm.nih.gov/sra/PRJNA1088925. The data generated in the present study may be requested from the corresponding author.

Authors' contributions

WJ, UJ, SG, HN, BL, SHK, SR, JiP and JoP contributed to conception and design. WJ, UJ, SG, HN, QH, SL and JoP acquired, analyzed and interpreted the data. WJ, UJ, SG and

HN participated in the data acquisition and analysis. SHK and JoP contributed the funding and performed the final revision of the manuscript. WJ and JoP confirm the authenticity of all the raw data. All authors agreed to be accountable for all aspects of the work, and all authors read and approved the final version of the manuscript.

Ethics approval and consent to participate

Experiments using human derivatives, materials, methods, ethical considerations and reasons for exemption from research subject consent were reviewed by the institutional review board of Chungnam National University Hospital, and exemption from review was approved on the condition that human derivatives were provided from a biobank (approval no. CNUH 2022-11-087; Daejeon, South Korea). The biospecimens and data used for this study were provided by the Biobank of Korea-CBNUH, a member of the Korea Biobank Network. Also, the Institutional Animal Care and Use Committee of Chungnam National University approved all animal management and experiment protocols (approval nos. 202305A-CNU-083 and 202309A-CNU-155). All mice experiments were conducted in animal facilities in accordance with institutional guidelines.

Patient consent for publication

Not applicable.

Competing interests

The authors declare that they have no competing interests.

References

1. Larsson L, Degens H, Li M, Salviati L, Lee YI, Thompson W, Kirkland JL and Sandri M: Sarcopenia: Aging-Related loss of muscle mass and function. Physiol Rev 99: 427-511, 2019.
2. Chianca V, Albano D, Messina C, Gitto S, Ruffo G, Guarino S, Del Grande F and Sconfienza LM: Sarcopenia: Imaging assessment and clinical application. Abdom Radiol (NY) 47: 3205-3216, 2022.
3. Geladari E, Alexopoulos T, Kontogianni MD, Vasilieva L, Mani I and Alexopoulou A: Mechanisms of sarcopenia in liver cirrhosis and the role of myokines. Ann Gastroenterol 36. 392-404, 2023.
4. Xu J, Wan CS, Ktoris K, Reijnierse EM and Maier AB: Sarcopenia is associated with mortality in adults: A systematic review and meta-analysis. Gerontology 68: 361-376, 2022.
5. Wahlen BM, Mekkodathil A, Al-Thani H and El-Menyar A: Impact of sarcopenia in trauma and surgical patient population: A literature review. Asian J Surg 43: 647-653, 2020.
6. Mirzai S, Eck BL, Chen PH, Estep JD and Tang WHW: Current approach to the diagnosis of sarcopenia in heart failure: A narrative review on the role of clinical and imaging assessments. Circ Heart Fail 15: e009322, 2022.
7. Fabian MR, Sonenberg N and Filipowicz W: Regulation of mRNA translation and stability by microRNAs. Annu Rev Biochem 79: 351-379, 2010.
8. Chekulaeva M and Filipowicz W: Mechanisms of miRNA-mediated post-transcriptional regulation in animal cells. Curr Opin Cell Biol 21: 452-460, 2009.
9. Filipowicz W, Bhattacharyya SN and Sonenberg N: Mechanisms of post-transcriptional regulation by microRNAs: Are the answers in sight? Nat Rev Genet 9: 102-114, 2008.
10. O'Brien J, Hayder H, Zayed Y and Peng C: Overview of MicroRNA biogenesis, mechanisms of actions, and circulation. Front Endocrinol (Lausanne) 9: 402, 2018.
11. Brzeszczynska J, Brzeszczynski F, Hamilton DF, McGregor R and Simpson AHRW: Role of microRNA in muscle regeneration and diseases related to muscle dysfunction in atrophy, cachexia, osteoporosis, and osteoarthritis. Bone Joint Res 9: 798-807, 2020.
12. Yanai K, Kaneko S, Ishii H, Aomatsu A, Ito K, Hirai K, Ookawara S, Ishibashi K and Morishita Y: MicroRNAs in Sarcopenia: A systematic review. Front Med (Lausanne) 7: 180, 2020.
13. Lee J and Kang H: Role of MicroRNAs and Long Non-Coding RNAs in Sarcopenia. Cells 11: 187, 2022.
14. Gan L and Denecke B: Profiling Pre-MicroRNA and Mature MicroRNA expressions using a single microarray and avoiding separate sample preparation. Microarrays (Basel) 2: 24-33, 2013.
15. Pan B, Yu J and Liu X: Upregulation of miR-886 indicates poor prognosis and promotes tumour progression of prostate cancer. Andrologia 54: e14296, 2022.
16. Lee K, Kunkeaw N, Jeon SH, Lee I, Johnson BH, Kang GY, Bang JY, Park HS, Leelayuwat C and Lee YS: Precursor miR-886, a novel noncoding RNA repressed in cancer, associates with PKR and modulates its activity. RNA 17: 1076-1089, 2011.
17. Lee H, Hong Y, Kong G, Lee DH, Kim M, Tran Q, Cho H, Kim C, Park S, Kim SH, *et al*: Yin Yang 1 is required for PHD finger protein 20-mediated myogenic differentiation in vitro and in vivo. Cell Death Differ 27: 3321-3336, 2020.
18. Livak KJ and Schmittgen TD: Analysis of relative gene expression data using real-time quantitative PCR and the 2(-Delta Delta C(T)) Method. Methods 25: 402-408, 2001.
19. Vo TT, Tran Q, Hong Y, Lee H, Cho H, Kim M, Park S, Kim C, Bayarmunkh C, Boldbaatar D, *et al*: AXL is required for hypoxia-mediated hypoxia-inducible factor-1 alpha function in glioblastoma. Toxicol Res 39: 669-679, 2023.
20. Tang Z, Kang B, Li C, Chen T and Zhang Z: GEPIA2: An enhanced web server for large-scale expression profiling and interactive analysis. Nucleic Acids Res 47: W556-W560, 2019.
21. GTEx Consortium: Human genomics. The Genotype-Tissue Expression (GTEx) pilot analysis: Multitissue gene regulation in humans. Science 348: 648-660, 2015.
22. Lee KP, Shin YJ, Panda AC, Abdelmohsen K, Kim JY, Lee SM, Bahn YJ, Choi JY, Kwon ES, Baek SJ, *et al*: miR-431 promotes differentiation and regeneration of old skeletal muscle by targeting Smad4. Genes Dev 29: 1605-1617, 2015.
23. Salant GM, Tat KL, Goodrich JA and Kugel JF: miR-206 knockout shows it is critical for myogenesis and directly regulates newly identified target mRNAs. RNA Biol 17: 956-965, 2020.
24. Iannone F, Montesanto A, Cione E, Crocco P, Caroleo MC, Dato S, Rose G and Passarino G: Expression Patterns of Muscle-Specific miR-133b and miR-206 correlate with nutritional status and Sarcopenia. Nutrients 12: 297, 2020.
25. Scott MS, Avolio F, Ono M, Lamond AI and Barton GJ: Human miRNA precursors with box H/ACA snoRNA features. PLoS Comput Biol 5: e1000507, 2009.
26. Scott MS, Ono M, Yamada K, Endo A, Barton GJ and Lamond AI: Human box C/D snoRNA processing conservation across multiple cell types. Nucleic Acids Res 40: 3676-3688, 2012.
27. Scott MS and Ono M: From snoRNA to miRNA: Dual function regulatory non-coding RNAs. Biochimie 93: 1987-1992, 2011.
28. Rother S and Meister G: Small RNAs derived from longer non-coding RNAs. Biochimie 93: 1905-1915, 2011.
29. Coley AB, DeMeis JD, Chaudhary NY and Borchert GM: Small nucleolar derived RNAs as regulators of human cancer. Biomedicines 10: 1819, 2022.
30. Purnamasari D, Tetrasiwi EN, Kartiko GJ, Astrella C, Husam K and Laksmi PW: Sarcopenia and chronic complications of type 2 diabetes mellitus. Rev Diabet Stud 18: 157-165, 2022.
31. Sabatino A, Cuppari L, Stenvinkel P, Lindholm B and Avesani CM: Sarcopenia in chronic kidney disease: What have we learned so far? J Nephrol 34: 1347-1372, 2021.
32. Owens J, Moreira K and Bain G: Characterization of primary human skeletal muscle cells from multiple commercial sources. In Vitro Cell Dev Biol Anim 49: 695-705, 2013.
33. Harding CP and Vargis E: Muscle atrophy marker expression differs between rotary cell culture system and animal studies. Biomed Res Int 2019: 2042808, 2019.
34. Kang SH, Lee HA, Kim M, Lee E, Sohn UD and Kim I: Forkhead box O3 plays a role in skeletal muscle atrophy through expression of E3 ubiquitin ligases MuRF-1 and atrogin-1 in Cushing's syndrome. Am J Physiol Endocrinol Metab 312: E495-E507, 2017.

35. Chan J, Lu YC, Yao MM and Kosik RO: Correlation between hand grip strength and regional muscle mass in older Asian adults: An observational study. BMC Geriatr 22: 206, 2022.
36. Bodine SC: Disuse-induced muscle wasting. Int J Biochem Cell Biol 45: 2200-2208, 2013.
37. Nunes EA, Stokes T, McKendry J, Currier BS and Phillips SM: Disuse-induced skeletal muscle atrophy in disease and nondisease states in humans: Mechanisms, prevention, and recovery strategies. Am J Physiol Cell Physiol 322: C1068-C1084, 2022.
38. Urso ML, Scrimgeour AG, Chen YW, Thompson PD and Clarkson PM: Analysis of human skeletal muscle after 48 h immobilization reveals alterations in mRNA and protein for extracellular matrix components. J Appl Physiol (1985) 101: 1136-1148, 2006.
39. Aihara M, Hirose N, Katsuta W, Saito F, Maruyama and Hagiwara H: A new model of skeletal muscle atrophy induced by immobilization using a hook-and-loop fastener in mice. J Phys Ther Sci 29: 1779-1783, 2017.
40. Shen Y, Zhang R, Xu L, Wan Q, Zhu J, Gu J, Huang Z, Ma W, Shen M, Ding F and Sun H: Microarray analysis of gene expression provides new insights into denervation-induced skeletal muscle atrophy. Front Physiol 10: 1298, 2019.
41. Spangenburg EE, Chakravarthy MV and Booth FW: p27Kip1: A key regulator of skeletal muscle satellite cell proliferation. Clin Orthop Relat Res (403 Suppl): S221-S227, 2002.
42. Pruitt SC, Freeland A, Rusiniak ME, Kunnev D and Cady GK: Cdkn1b overexpression in adult mice alters the balance between genome and tissue ageing. Nat Commun 4: 2626, 2013.
43. Toklowicz M, Zbikowska A, Janusz P, Kotwicki T, Andrusiewicz M and Kotwicka M: MicroRNA expression profile analysis in human skeletal muscle tissue: Selection of critical reference. Biomed Pharmacother 162: 114682, 2023.
44. Mytidou C, Koutsoulidou A, Katsioloudi A, Prokopi M, Kapnisis K, Michailidou K, Anayiotos A and Phylactou LA: Muscle-derived exosomes encapsulate myomiRs and are involved in local skeletal muscle tissue communication. FASEB J 35: e21279, 2021.
45. Ma G, Wang Y, Li Y, Cui L, Zhao Y, Zhao B and Li K: MiR-206, a key modulator of skeletal muscle development and disease. Int J Biol Sci 11: 345-352, 2015.
46. Giagnorio E, Malacarne C, Mantegazza R, Bonanno S and Marcuzzo S: MyomiRs and their multifaceted regulatory roles in muscle homeostasis and amyotrophic lateral sclerosis. J Cell Sci 134: jcs258349, 2021.
47. Zhelankin AV, Iulmetova LN, Ahmetov II, Generozov EV and Sharova EI: Diversity and Differential Expression of MicroRNAs in the human skeletal muscle with distinct fiber type composition. Life (Basel) 13: 659, 2023.
48. Powers SK, Lynch GS, Murphy KT, Reid MB and Zijdewind I: Disease-Induced skeletal muscle atrophy and fatigue. Med Sci Sports Exerc 48: 2307-2319, 2016.
49. Sartori R, Romanello V and Sandri M: Mechanisms of muscle atrophy and hypertrophy: Implications in health and disease. Nat Commun 12: 330, 2021.
50. Marusic U, Narici M, Simunic B, Pisot R and Ritzmann R: Nonuniform loss of muscle strength and atrophy during bed rest: A systematic review. J Appl Physiol (1985) 131: 194-206, 2021.
51. Gao Y, Arfat Y, Wang H and Goswami N: Muscle atrophy induced by mechanical unloading: Mechanisms and potential countermeasures. Front Physiol 9: 235, 2018.
52. Hosoyama T, Van Dyke J and Suzuki M: Applications of skeletal muscle progenitor cells for neuromuscular diseases. Am J Stem Cells 1: 253-263, 2012.
53. Pang KT, Loo LSW, Chia S, Ong FYT, Yu H and Walsh I: Insight into muscle stem cell regeneration and mechanobiology. Stem Cell Res Ther 14: 129, 2023.
54. Ji LL and Yeo D: Mitochondrial dysregulation and muscle disuse atrophy. F1000Res 8: F1000 Faculty Rev-1621, 2019.
55. Manas-Garcia L, Penedo-Vazquez A, Lopez-Postigo A, Deschrevel J, Duran X and Barreiro E: Prolonged immobilization exacerbates the loss of muscle mass and function induced by cancer-associated cachexia through enhanced proteolysis in mice. Int J Mol Sci 21: 8167, 2020.
56. Thompson JM, West DWD, Doering TM, Budiono BP, Lessard SJ, Koch LG, Britton SL, Byrne NM, Brown MA, Ashton KJ and Coffey VG: Effect of short-term hindlimb immobilization on skeletal muscle atrophy and the transcriptome in a low compared with high responder to endurance training model. PLoS One 17: e0261723, 2022.
57. Kim H, Bae YU, Lee H, Kim H, Jeon JS, Noh H, Han DC, Byun DW, Kim SH, Park HK, et al: Effect of diabetes on exosomal miRNA profile in patients with obesity. BMJ Open Diabetes Res Care 8: e001403, 2020.
58. Hata J, Nakashima D, Tsuji O, Fujiyoshi K, Yasutake K, Sera Y, Komaki Y, Hikishima K, Nagura T, Matsumoto M, et al: Noninvasive technique to evaluate the muscle fiber characteristics using q-space imaging. PLoS One 14: e0214805, 2019.
59. Wang C, Yue F and Kuang S: Muscle histology characterization using H&E staining and muscle fiber type classification using immunofluorescence staining. Bio Protoc 7: e2279, 2017.